crystals

MDPI

Article

Synthesis, X-ray Crystal Structure and Antimicrobial Activity of Unexpected Trinuclear Cu(II) Complex from *s*-Triazine-Based Di-Compartmental Ligand via Self-Assembly

Saied M. Soliman [1,*], Jamal Lasri [2], Matti Haukka [3], Essam N. Sholkamy [4], Hessa H. Al-Rasheed [5] and Ayman El-Faham [1,5,*]

1 Department of Chemistry, Faculty of Science, Alexandria University, P.O. Box 426, Ibrahimia, Alexandria 21321, Egypt
2 Department of Chemistry, Rabigh College of Science and Arts, King Abdulaziz University, P.O. Box 344, Jeddah 21589, Saudi Arabia; jlasri@kau.edu.sa
3 Department of Chemistry, University of Jyväskylä, P.O. Box 35, FI-40014 Jyväskylä, Finland; matti.o.haukka@jyu.fi
4 Department of Botany and Microbiology, College of Science, King Saud University, P.O. Box 2455, Riyadh 11451, Saudi Arabia; essam_92003@yahoo.com
5 Department of Chemistry, College of Science, King Saud University, P. O. Box 2455, Riyadh 11451, Saudi Arabia; halbahli@Ksu.edu.sa
* Correspondence: saied1soliman@yahoo.com (S.M.S.); aymanel_faham@hotmail.com (A.E.-F.)

Received: 20 November 2019; Accepted: 5 December 2019; Published: 9 December 2019

Abstract: The synthesis and X-ray crystal structure of the trinuclear $[Cu_3(HL)(Cl)_2(NO_3)(H_2O)_5](NO_3)_2$ complex of the *s*-triazine-based di-compartmental ligand, 2-methoxy-4,6-*bis*(2-(pyridin-2-ylmsethylene)hydrazinyl)-1,3,5-triazine (H_2L), are presented. The Cu1 and Cu2 are penta-coordinated with CuN_3ClO coordination environment, distorted square pyramidal coordination geometry while Cu3 is hexa-coordinated with CuN_2O_4 coordination sphere, and distorted octahedral geometry. The complex crystallized in the primitive P-1 triclinic crystal system with two molecular units per unit cell. Its packing is dominated by the O–H (35.5%) and Cl–H (8.8%) hydrogen bonding interactions as well as the π–π stacking (2.3%) and anion–π-stacking interactions (3.7%). The different coordination interactions were analyzed using atoms in molecules (AIM) theory, and the number of charge transferences from the ligand group to Cu(II) were determined using natural bond orbital calculations. The effect of the free ligand and its Cu(II) complex on the tested pathogenic microbes (*Staphylococcus aureus*, *S. epidermidis*, *Enterococcus faecalis*, *Escherichia coli*, *Salmonella typhi* and *Pseudomonas aeruginosa*) and one fungal isolate (*Candida albicans)* is presented. Both have wide spectrum antimicrobial activity against the selected microorganism. It is observed that the free ligand at 180 µg/mL was more effective than its Cu(II) complex and showed close results compared to the positive control gentamicin. At higher concentrations (1 mg/mL), the Cu(II) complex was found to be more active against *S. epidermidis*, *E. coli* and *C. albicans* than the lower concentration. The minimum inhibitory concentration (MIC) and minimum bactericidal concentration (MBC) values are also lower for the Cu(II) complex than the free ligand.

Keywords: *s*-Triazine; trinuclear; Hirshfeld; antimicrobial; NBO

1. Introduction

s-Triazine-based ligands with two hydrazone arms (Figure 1) are versatile building blocks used to construct interesting mononuclear, dinuclear and polynuclear metal complexes. In literature,

these ligands have structure duality [1–15]. They can form mononuclear pincer complexes when the two-ligand arms are located in the same direction (mode A). They can also act as di-compartmental ligands if one of these arms is rotated along the N–N bond leading to dinuclear metal complexes (mode B). In these cases, the interaction with the *s*-triazine ligand is called either pyridine or pyrimidine-like coordination behavior, respectively [10]. Factors that control the ligand behavior are the nature of ligating atoms, metal ion size and charge as well as the nature of solvent used [1–7]. The complexation of Co(II), Hg(II) and Pb(II) [10–12] with *bis*-tridentate *s*-triazine chelates was investigated by Lehn and co-workers. Recently, the Mn(II) and Cd(II) complexes of the H_2L ligand (Figure 1) using self-assembly was reported by our research group [13,14]. More recently and with the same synthetic strategy, we also reported two di-compartmental metal(II) complexes with Co(II) and Ni(II) [15] where the metal ion size was the critical factor that controlled the ligand behavior in these cases [13–15]. In view of the interesting and versatile coordination behavior of this ligand, we present a new rare case of Cu(II) complex with the same di-compartmental ligand. The structure of the new complex was identified using single crystal X-ray diffraction, and the molecular packing interactions were discussed based on Hirshfeld surface analysis. Its structure aspect was analyzed using Density functional theory (DFT) calculations. Moreover, its antimicrobial activity was determined and compared with the free ligand (H_2L).

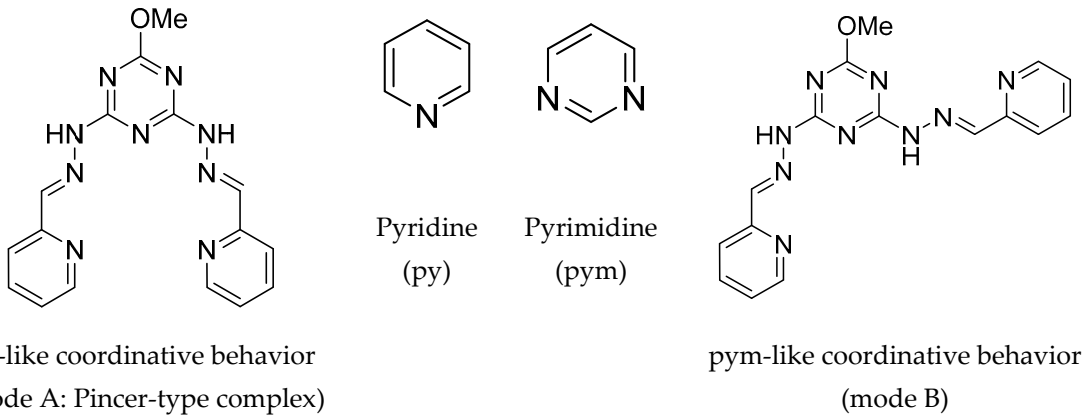

Figure 1. The possible coordination behaviors of the ligand (H_2L).

2. Materials and Methods

2.1. Materials and Physical Measurements

Solvent and reagents were purchased from Sigma-Aldrich (Sigma-Aldrich Chemie GmbH, 82024 Taufkirchen, Germany) and were used without further purification. The CHN analyses were determined using PerkinElmer 2400 elemental analyzer (PerkinElmer, Inc.940 Winter Street, Waltham, MA, USA).

2.2. Synthesis of $[Cu_3(HL)(Cl)_2(NO_3)(H_2O)_5](NO_3)_2$ (**1**)

The ligand was prepared by following the method described by our research group [13,14]. A 10 mL methanolic solution of H_2L (0.349 g, 1 mmol) was mixed with an aqueous solution (5 mL) of copper(II) chloride (0.135 g, 1 mmol) followed by addition of 3 drops of diluted nitric acid HNO_3 (1:1 *v*/*v*). This mixture was left to slowly evaporate at room temperature; $[Cu_3(HL)(Cl)_2(NO_3)(H_2O)_5](NO_3)_2$ (**1**) complex was obtained as blue crystals after three weeks.

Yield; $C_{16}H_{24}Cl_2Cu_3N_{12}O_{15}$: 72%. Anal. Calc. (%): C, 21.69; H, 2.73; N, 18.97; Found: C, 21.77; H, 2.80; N, 18.75.

2.3. X-ray Structure Determination

The crystal of $[Cu_3(HL)(Cl)_2(NO_3)(H_2O)_5](NO_3)_2$ (**1**) was measured using Rigaku Oxford Diffraction Supernova diffractometer using Mo Kα (λ = 0.71073 Å) radiation at 120 K. The CrysAlisPro [16] program package and the *SHELXT* [17] software were used for solving and refine the structure with the aid of *Olex2* [18] graphical user interface (See Supplementary data). The crystallographic details are summarized in Table 1.

Table 1. Crystal data of **1**.

	1
empirical formula	$C_{16}H_{24}Cl_2Cu_3N_{12}O_{15}$
Fw	885.99
temp (K)	120(2) K
λ (Å)	0.71073
crystal system	Triclinic
space group	P-1
a (Å)	7.1252(3)
b (Å)	13.2067(5)
c (Å)	16.0792(7)
a (deg)	94.059(4)
β (deg)	101.947(4)
γ (deg)	92.712(3)
V (Å^3)	1473.59(11)
Z	2
ρ_{calc} (Mg/m^3)	1.997
μ(Mo Kα) (mm^{-1})	2.418
number of reflections	14,147
unique reflections	7983
GOOF (F^2) *	1.050
R_{int}	0.0267
R1 [a] ($I \geq 2\sigma$)	0.0476
wR2 [b] ($I \geq 2\sigma$)	0.1099
CCDC **	1,965,390

[a] $R1 = \Sigma||F_o| - |F_c||/\Sigma|F_o|$. [b] $wR2 = [\Sigma[w(F_o^2 - F_c^2)^2]/ \Sigma[w(F_o^2)^2]]^{1/2}$. * Goodness of fit; ** CCDC = Cambridge Crystallographic Data Centre Number

2.4. Hirshfeld Surface Analysis

The topology analyses were performed using Crystal Explorer 17.5 program [19] in order to determine the percentages of the different intermolecular interactions in the crystal structure of the studied Cu(II) complex.

2.5. Computational Details

With the aid of Gaussian 09 program package [20,21], single point calculations employing the MPW1PW91 [22] method combined with the TZVP basis sets for all atoms were performed. Natural atomic charges were calculated using natural bond order (NBO) calculations with the aid of NBO program [23], while Multiwfn [24] program was used to compute the atoms in molecules (AIM) topological parameters.

2.6. Antimicrobial Experiments

2.6.1. Test Microorganism

The antibacterial activity of H_2L and its Cu(II) complex was assessed against two bacteria groups: Gram-positive bacteria namely; *S. aureus ATCC* 29213, *S. epidermidis ATCC 12228* and *E. faecalis ATCC* 29212 and Gram-negative bacteria, namely *E. coli ATCC 25922, P. aeruginosa ATCC 27853* and

S. typhimurium ATCC 14028, maintained in brain heart infusion (BHI) broth at 20 °C; 300 mL of each stock culture was added to 3 mL of BHI broth. Overnight cultures were kept for 24 h at 37 ± 1 °C, and the purity of cultures was checked after 24 h of incubation. The bacterial suspension (inoculum) was diluted with sterile physiological solution to 10^8 CFU/mL (turbidity = McFarland barium sulfate standard 0.5). In case of fungus *C. albicans ATCC 60193*, the used medium in antagonistic activity against tested fungi was potato dextrose agar (PDA) [25].

2.6.2. Well Diffusion Method for Showing Antimicrobial Activity

Solutions of H_2L and its Cu(II) complex (**1**) were prepared at a concentration of 3 mg/mL in DMSO as stock solution. Sterilized Mueller–Hinton agar plates seeded with pathogenic bacteria were prepared and 60 µL of stock solution was added in wells according to the well diffusion method [25]. The plates were incubated at 37 °C for 24 h, and the antimicrobial activity was determined by measuring the inhibition zones. Gentamicin was used as positive control in the all experiments.

2.6.3. Minimum Inhibitory Concentration (MIC) Determination

The antibacterial activity of H_2L and its Cu(II) complex (**1**) was studied by employing micro-dilution method using Mueller–Hinton broth [26]. Stock solutions (3 mg/ml) of H_2L and **1** were prepared in DMSO as solvent. Further 1:2 serial dilutions were performed by addition of culture broth to reach concentrations ranging from 1.5 to 0.235 mg/mL. The 90 µL of medium was distributed in 96–well plates, as well as a sterility control and a growth control (containing culture broth plus DMSO, without antimicrobial substance). Each test and growth control well was inoculated with 10 µl of the bacterial suspension (10^8 CFU/mL) and then incubated at 37 °C for 24 h. The culture broth at each dilution inoculated on nutrient agar was used to detect MIC and minimum bactericidal concentration (MBC) [27–30].

3. Results and Discussion

3.1. X-ray Structure Description

The trinuclear $[Cu_3(HL)(Cl)_2(NO_3)(H_2O)_5](NO_3)_2$ (**1**) complex crystallized in the triclinic primitive P-1 space group with one asymmetric unit and two molecular formula units per unit cell. A list of the bond distances and angles is summarized in Table 2 while the structure of the asymmetric unit is shown in Figure 2. In the course of preparation, the hydrazone NH proton of one of the two ligand arms was abstracted leading to the mononegative polydentate ligand (HL^-), which comprised nine nitrogen atoms. Of these N-sites, there are eight nitrogen atoms coordinating to the three copper centers. The Cu1 and Cu2 centers are penta-coordinated and with very similar coordination environment. In both cases, the Cu(II) is coordinated with one water molecule, one chloride ion and the three nitrogen atoms from the organic ligand: (i) the pyridyl, (ii) the hydrazone CH=N and (iii) one of the *s*-triazine nitrogen atoms. The Cu1–N1, Cu1–N2 and Cu1–N6 distances are 2.041(3), 1.964(3) and 2.062(3) Å, respectively, and the Cu2–N9, Cu2–N8 and Cu2–N4 distances are 2.006(3), 1.965(3) and 2.027(3) Å, respectively. Generally, the strength of Cu–N interactions increased in the order of $Cu–N_{triazine} < Cu–N_{pyridine} < Cu–N_{hydrazone}$. The Cu1–Cl1 (2.233(9) Å) and Cu2–Cl2 (2.216(10) Å) are slightly different from each other. The Cu1–O1 (2.307(3) Å) and Cu2–O3 (2.391(3) Å) are not equivalent. The coordination geometry around these Cu(II) centers could be described as distorted square pyramid where the three nitrogen atoms and the coordinated chloride ion forming the base and the oxygen of the coordinated water molecule are at the apex. On other hand, the Cu3 is hexa-coordinated with CuN_2O_4 coordination environment. The organic ligand is coordinated to Cu3 via two nitrogen atoms; one from the *s*-triazine ring with long Cu3–N5 distance of 2.730(3) Å and the other from the negatively charged N-site from the de-protonated hydrazone NH group with Cu3–N7 distance of 2.002(3) Å. In addition, the highly distorted octahedral configuration of Cu3 is completed by four oxygen atoms from three water molecules and one nitrate ion as monodentate ligands. The base of the distorted

octahedron comprised the two Cu–N interactions as well as the Cu3–O6 (1.967(3) Å) and Cu3–O7 (2.301(3) Å) bonds while the apical positions are occupied by two axial water molecules with almost identical Cu3–O4 and Cu3–O5 distances of 1.950(3) and 1.946(3) Å, respectively.

Table 2. Selected bond lengths (Å) and angles (°) for $[Cu_3(HL)(Cl)_2(NO_3)(H_2O)_5](NO_3)_2$ (**1**) complex.

Bond Distances			
Cu1–N2	1.964(3)	Cu2–Cl2	2.216(10)
Cu1–N1	2.041(3)	Cu2–O3	2.391(3)
Cu1–N6	2.062(3)	Cu3–O5	1.946(3)
Cu1–Cl1	2.233(9)	Cu3–O4	1.950(3)
Cu1–O1	2.307(3)	Cu3–O6	1.967(3)
Cu2–N8	1.965(3)	Cu3–N7	2.002(3)
Cu2–N9	2.006(3)	Cu3–N5	2.730(3)
Cu2–N4	2.027(3)	Cu3–O7	2.301(3)
Bond Angles			
N2–Cu1–N1	79.11(12)	N4-Cu2–Cl2	103.36(9)
N2–Cu1–N6	78.19(12)	N8–Cu2–O3	86.79(11)
N1–Cu1–N6	157.28(12)	N9–Cu2–O3	99.63(11)
N2–Cu1–Cl1	168.21(9)	N4-Cu2–O3	87.40(11)
N1–Cu1–Cl1	96.97(9)	Cl2-Cu2–O3	97.89(7)
N6-Cu1–Cl1	105.13(8)	O5–Cu3–O4	174.67(13)
N2–Cu1–O1	86.64(11)	O5–Cu3–O6	84.02(19)
N1–Cu1–O1	87.67(11)	O4–Cu3–O6	90.67(19)
N6-Cu1–O1	91.86(11)	O5–Cu3–N7	90.58(12)
Cl1-Cu1–O1	104.40(7)	O4–Cu3–N7	94.18(12)
N8–Cu2–N9	80.46(12)	O6-Cu3–N7	157.47(18)
N8–Cu2–N4	78.43(11)	O5–Cu3–O7	90.82(13)
N9–Cu2–N4	157.32(12)	O4–Cu3–O7	90.81(14)
N8–Cu2–Cl2	175.03(9)	O6-Cu3–O7	103.30(17)
N9–Cu2–Cl2	97.04(9)	N7-Cu3–O7	98.62(11)

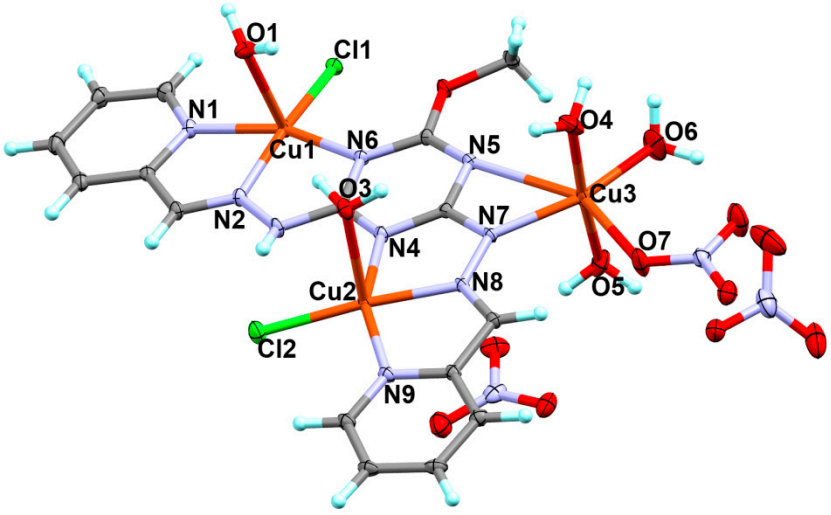

Figure 2. Thermal ellipsoids at 30% probability and atom numbering scheme of the asymmetric unit of $[Cu_3(HL)(Cl)_2(NO_3)(H_2O)_5](NO_3)_2$ (**1**) complex.

The complex molecules are packed in the three dimensional structure via a complicated set of intermolecular O–H hydrogen bonding interactions (Figure 3). In addition to the two weak non-classical C4–H4–O9 (3.192(5) Å) and C6–H6–O3 (3.199(4) Å) hydrogen bonding interactions, the complex units are packed by many strong O–H–O hydrogen bonding interactions between the coordinated water molecule as hydrogen bond donor and nitrate anions as hydrogen bond acceptor with donor-acceptor

distances ranging from 2.641(4) to 3.184(4) Å for the O5–H5A–O10 and O1–H1B–O15 hydrogen bonds, respectively. A view of molecular packing is presented in Figure 4, and the details of the hydrogen bond parameter are summarized in Table 3.

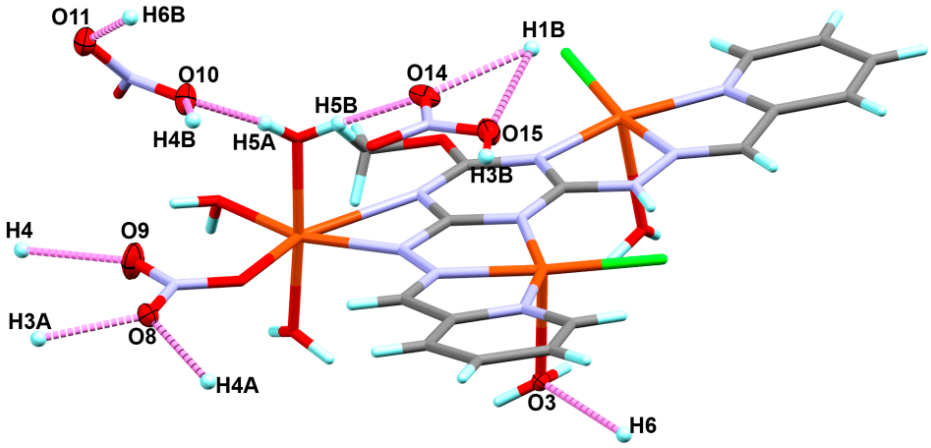

Figure 3. The most important hydrogen bond contacts included in the molecular packing of the studied Cu(II) complex.

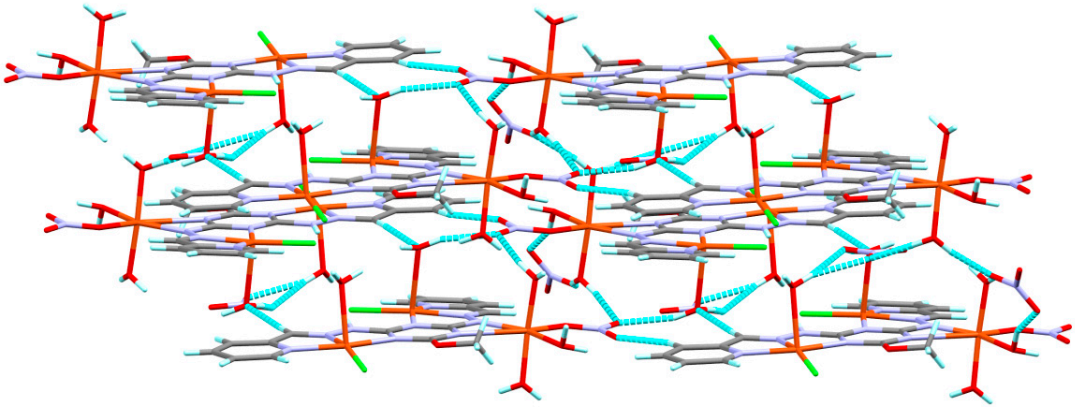

Figure 4. Packing of the complex units by intermolecular O–H–O and C–H–O hydrogen bonding interactions.

Table 3. Hydrogen bonds for $[Cu_3(HL)(Cl)_2(NO_3)(H_2O)_5](NO_3)_2$ (**1**) complex (Å and °).

D–H–A	d(D–H)	d(H–A)	d(D–A)	<(DHA)
O1–H1B–O14#1	0.84	2.15	2.929(4)	153.1
O1–H1B–O15#1	0.84	2.43	3.184(4)	149.1
O3–H3A–O8#2	0.87	2.06	2.910(4)	165.2
O3–H3B–O15#1	0.93	2.05	2.895(5)	150.0
O4–H4A–O8#2	0.86	1.91	2.728(4)	159.9
O4–H4B–O10#1	0.89	1.92	2.766(4)	157.2
O5–H5A–O10	0.83	1.82	2.641(4)	172.0
O5–H5B–O14	0.87	1.85	2.715(5)	174.2
O6-H6B–O11#1	0.89	1.87	2.698(6)	153.4
C4–H4–O9#3	0.95	2.3	3.192(5)	156.6
C6–H6–O3#4	0.95	2.26	3.199(4)	168.1

#1 x + 1, y, z; #2 –x + 3, –y + 1, –z; #3 x + 1, y, z + 1; #4 –x + 4, –y + 1, –z + 1.

3.2. Hirshfeld Analysis

The intermolecular interactions in the crystal structure of the trinuclear complex unit $[Cu_3(HL)(Cl)_2(NO_3)(H_2O)_5]^{2+}$ were analyzed using Hirshfeld topology analysis. All intermolecular

contacts and their percentages are presented graphically in Figure 5. In addition to the H–H contacts (23.4%), the polar O–H (35.5%) and Cl–H (8.8%) hydrogen bonds are considered not only the strongest contacts but also the most important in the molecular packing of the complex units (Figure 6). The O–H and Cl–H fingerprint plots showed sharp spikes with many red spots of different intensities in the d_{norm} map indicating that these interactions are strong and short compared with the van der Waals radii sum of the two elements. Presentation of these interactions for the $[Cu_3(HL)(Cl)_2(NO_3)(H_2O)_5]^{2+}$ complex ion with the neighboring units are mapped based on d_{norm} Hirshfeld surface and shown in Figure 7. There are some interactions between the coordinated chloride anion and the nitrate counter anion with the organic ligand C and N-atoms. The Cl1–N2 interaction distance is 3.293 Å, which contributed by 1.9% from the whole fingerprint area while the nitrate counter anion to the organic ligand intermolecular distances are the shortest for C8–O14 (3.160 Å), C11–O13 (2.998 Å) and N8–N12 (3.031 Å) with one nitrate anion while C7–O15 (3.145 Å), C8–O13 (3.171 Å) and C9–O14 (3.183 Å) with the other nitrate counter anion. The net amount of these anion–π-stacking interactions is 3.7% from the whole fingerprint area. The shortest C–C contact (2.3%) occurred between two pyridine moieties from two complex units with interaction distance of 3.333 Å for the C5–C16 contact indicating some weak π–π stacking interactions with characteristics blue/red triangle in the shape index map (Figure 8).

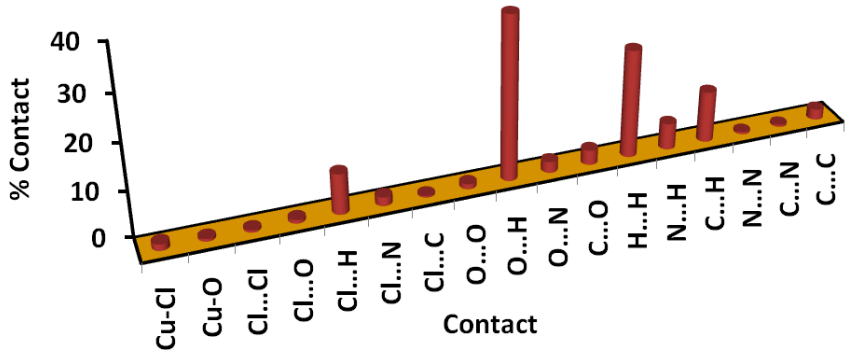

Figure 5. The intermolecular contacts and their percentages for the $[Cu_3(HL)(Cl)_2(NO_3)(H_2O)_5]^{2+}$ complex unit.

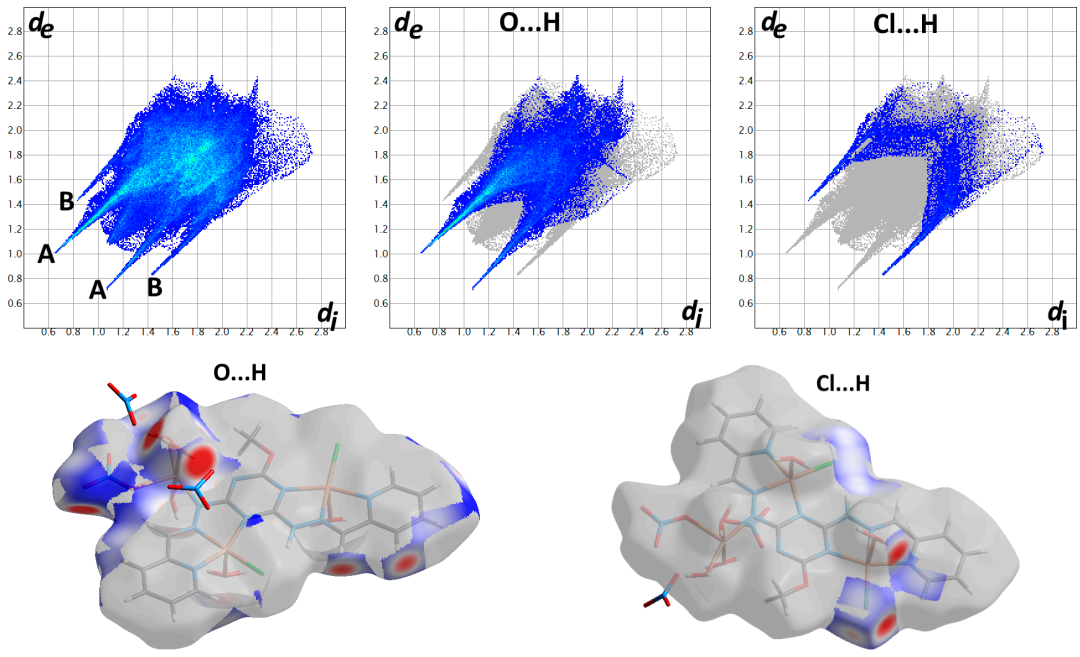

Figure 6. The full and decomposed fingerprint plots (upper) and decomposed d_{norm} maps (lower) of the O–H and Cl–H contacts in the $[Cu_3(HL)(Cl)_2(NO_3)(H_2O)_5]^{2+}$ unit.

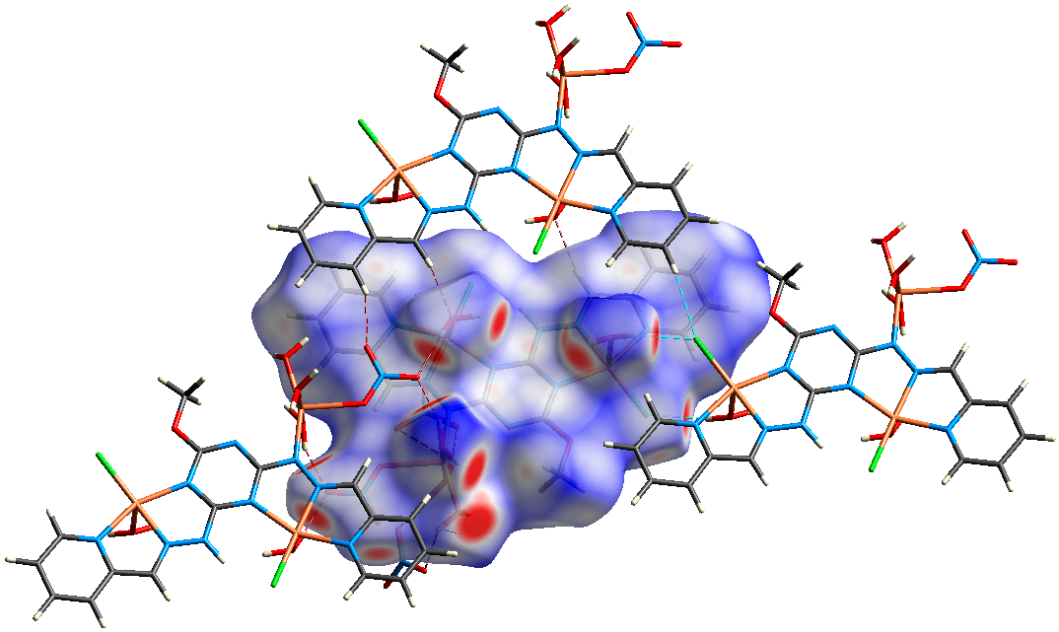

Figure 7. The O–H (brown dotted line) and Cl–H (turquoise dotted line) hydrogen bonds among the complex molecular units based on Hirshfeld analysis.

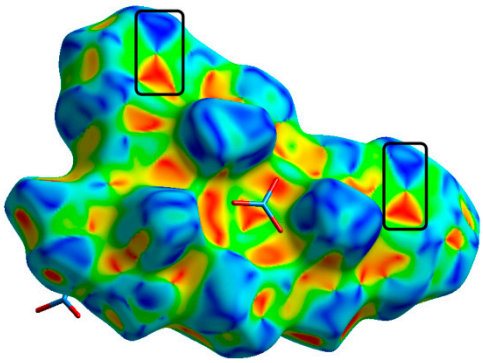

Figure 8. Shape index map showing the red/blue triangles at the pyridine moiety corresponding to the π–π stacking interactions.

3.3. DFT Studies

3.3.1. AIM Topology Analysis

The present section aims to shed light on the nature and strength of the Cu–N, Cu–Cl and Cu–O interactions in the studied complex [31–39]. A list of the calculated topological parameters is given in Table S1. The electron density (ρ(r)) values of the Cu–N, Cu–Cl and Cu–O interactions are in the range of 0.0739–0.0954, 0.0773–0.0774 and 0.0317–0.0858 a.u., respectively. The ρ(r) values for the Cu–N coordinate bonds with the hydrazone N-atom are the highest for Cu1 and Cu2 atoms. The values are very close to 0.1 a.u. indicating more covalent characters and stronger bonds for these interactions compared to the Cu–N(pyridine) and Cu–N(triazine). The Cu–N(triazine) bonds seems to be the weakest and have the least covalent character. It is clear from Figure 9 that the Cu–O and Cu–N interaction distances correlated very well with ρ(r) and the calculated interactions energies ($E_{int.}$) [39]. The Cu1–O1 and Cu2–O3 interactions with the axial water molecules as well as the Cu3–O7 interaction with the nitrate ion have the lowest ρ(r) values and are the weakest Cu–O interactions. The weak Cu1–O1 and Cu2–O3 interactions could be explained on the basis of the strong interactions between the Cu(II) center with the organic ligand as *NNN*-chelate and with the chloride anion in the equatorial

plane. This significantly weakens its interaction with the axial water molecule as a result of the strong charge compensation at the metal ion site. Another conclusion could be deduced from these results; the majority of the Cu–X (X = Cl, O or N) interactions have negative total energy density (H(r)) and potential to kinetic energy density (V(r)/G(r)) ratios more than 1 indicating the significant covalent characteristics of these interactions.

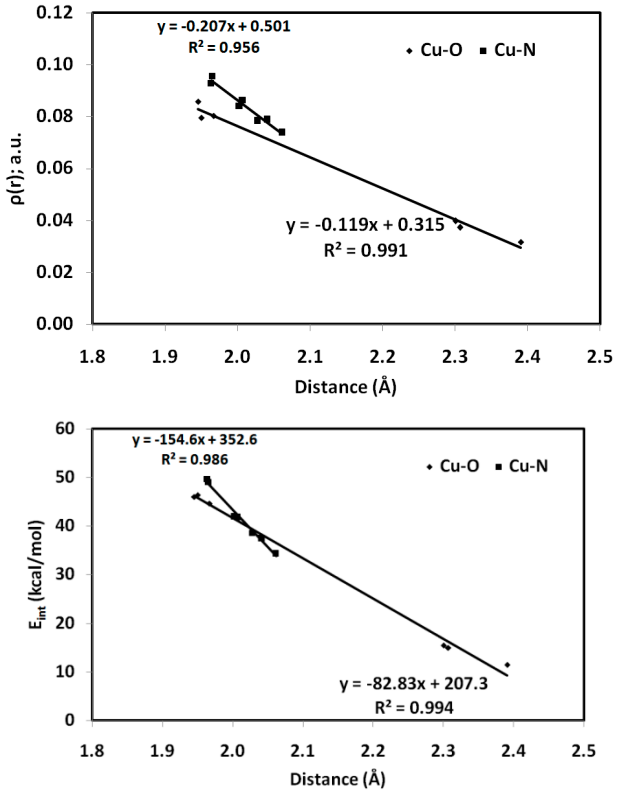

Figure 9. Correlations between the Cu–N/Cu–O distances with ρ(r) and $E_{int.}$ [39].

3.3.2. Natural Population Analysis

The natural charge populations at the different copper centers and also at the different ligand groups are collected in Table 4. In this trinuclear Cu(II) complex, the three copper centers have two different coordination environments. While Cu1 and Cu2 have almost square pyramidal coordination (CuN_3ClO) geometry with five coordinating sites, the Cu3 is hexa-coordinated with CuN_2O_4 coordination environment. From this point of view, the Cu1 and Cu2 have almost similar natural charges. The Cu1 and Cu2 natural charges are 0.830 and 0.838 e, respectively, while the corresponding value for Cu3 is 1.014 e, as its positive charge is less compensated by the electron density transferred from the coordinated ligand groups. The significant charge compensations that occurred at the Cu1 and Cu2 centers are mainly attributed to the coordinated chloride anion. The amount of electron density transferred from this coordinated anion to the Cu1 and Cu2 ions are 0.481 and 0.410 e, respectively. On the other hand, the coordinated water molecules transferred only 0.080 and 0.068 e to these copper centers, respectively. For Cu3, the nitrate anion, which is considered as a weaker electron donor compared to the chloride anion, transferred only 0.145 e while the three water molecules transferred a net of 0.521 e to this copper center. Interestingly, the coordinated mono-negative organic ligand (HL^-) has a net charge of 0.486 e indicating a significant number of electrons (1.486 e) transferred from the organic ligand to the three copper centers.

Table 4. The natural charges at the Cu sites and ligand groups.

Atom or Ligand Group	Charge
Cu1	0.8297
$H_2O(1)$	0.0805
Cl1	−0.5191
Cu2	0.8378
$H_2O(3)$	0.0682
Cl2	−0.5905
Cu3	1.0141
$H_2O(4)$	0.1602
$H_2O(5)$	0.1892
$H_2O(6)$	0.1717
$N(10)O_3^-$	−0.8550
$N(11)O_3^-$	−0.9484
$N(12)O_3^-$	−0.9243
HL^-	0.4860

3.4. Antimicrobial Activity of H_2L and its Cu(II) Complex

The effect of the free ligand H_2L and its Cu(II) complex on the tested pathogenic microbes is shown in Figure S1. Both showed wide spectrum antimicrobial activity against Gram-positive and Gram-negative bacteria as well as the fungus *C. albicans* (Table 5). It is observed that H_2L at 180 µg/mL was more effective than its Cu(II) complex and showed close results compared to the positive control gentamicin. At higher concentrations (1 mg/mL), the Cu(II) complex was found to be more active against *Streptococcus epidermidis, E. coli and C. albicans* than the lower concentration as shown form the results obtained in Table 6.

Table 5. The inhibition zone diameter (mm) for H_2L and its Cu(II) complex against target pathogenic microbes at 180 µg/mL per well.

Target microbes	Cu(II) Complex	H_2L	Gentamicin [a]
S. aureus	16	34	34
Streptococcus epidermidis	16	22	32
Enterococcus faecalis	9	13	21
E. coli	10	14	21
S. typhi	12	11	22
Pseudomonas aeruginosa	17	17	19
C. albicans	7	7	-

[a] 30 µg per disc.

Table 6. Minimum inhibitory (MIC) and minimum bactericidal concentration (MBC) in mg/mL for the Cu(II) complex and H_2L free ligand against *S. epidermidis*, *E. coli* and *C. albicans* growth.

Microbes	Complex 1 [a]	H_2L [a]
E. coli	0.375(0.563)	0.750 (1.125)
S. epidermidis	0.188 (0.282)	0.375 (0.563)
C. albicans	0.188 (0.282)	0.750 (1.125)

[a] MIC(MBC).

MICs and MBCs were determined for H_2L and its Cu(II) complex against *E. coli*, *S. epidermidis* and *C. albicans* (Table 6 and Figure S2). The Cu(II) complex showed strong bioactivity against the tested pathogenic microbes, more than the free ligand (H_2L). The effect of the Cu(II) complex against *S. epidermidis* as Gram-positive bacteria and the fungus *C. albicans* was found to be higher compared to the Gram-negative bacteria (*E. coil*). The free H_2L ligand activity was the highest against *S. epidermidis*

as Gram-positive bacteria compared to *E. coli* and *C. albicans*. Generally, the bioactivity of the Cu(II) complex against target microbes was found to be considerably more effective than the H_2L ligand as indicated by the low MIC and MBC values of the complex **1** compared to the free ligand (Table 6)

4. Conclusions

A novel coordination behavior of the di-compartmental ligand (H_2L) was observed with Cu(II) ion. The $[Cu_3(HL)(Cl)_2(NO_3)(H_2O)_5](NO_3)_2$ (1) complex is trinuclear with three Cu(II) centers coordinating the ligand in its anionic form (HL^-). The CuN_3ClO coordination environment of Cu1 and Cu2 has square pyramidal coordination configuration while the CuN_2O_4 coordination sphere of Cu3 has a distorted octahedral geometry. Hirshfeld analysis was used to quantitatively analyze the intermolecular interactions in the molecular packing of the Cu(II) complex. AIM calculations were also presented to shed light on the strength and nature of the Cu–Cl, Cu–O and Cu–N interactions while NBO method was used to predict the charge transferences from the ligand groups to Cu(II). The bioactivity of the free ligand (**H_2L**) and its Cu(II) complex (**1**) as antimicrobial agents was investigated. Both showed high antimicrobial activities against the selected microorganism. The results indicated that the Cu(II) complex has lower MIC and MBC values compared to the free ligand, indicating the higher potency of the Cu(II) complex as a antimicrobial agent compared to the free ligand.

Supplementary Materials: The following are available online at http://www.mdpi.com/2073-4352/9/12/661/s1, Figure S1: Growth inhibition images of target pathogenic microbes with the Cu(II) complex (**1**) and H2L, negative control DMSO alone (**C**), positive control, gentamicin, Figure S2: Photography images of inhibition of pathogenic microbe's growth at different concentrations of synthetic compounds to determine their MIC and MBC; the Cu(II) complex (**1**) and H2L, Table S1: Atoms in molecules (AIM) topological parameters (a.u.) of the Cu–N, Cu–Cl and Cu–O interactions.

Author Contributions: Synthesis of the ligand was carried out by H.H.A.-R. Synthesis of the complex and its X-ray study were carried out by S.M.S., J.L. and M.H. Biological activity was carried out by E.N.S. The work was designed and supervised by A.E.-F. and S.M.S. The results of the work and discussions were carried by all authors. The final version included contributions from all authors.

Funding: This research received no external funding.

Acknowledgments: The authors extend their appreciation to the Deanship of Scientific Research at King Saud University for funding this work through research group No (RGP-234, Saudi Arabia).

Conflicts of Interest: The authors declare no conflict of interest.

References

1. Lehn, J.M. Programmed Chemical Systems: Multiple Subprograms and Multiple Processing/Expression of Molecular Information. *Chem. Eur. J.* **2000**, *6*, 2097–2102. [CrossRef]
2. Lehn, J.M. Toward complex matter: Supramolecular chemistry and self-organization. *Proc. Natl. Acad. Sci. USA* **2002**, *99*, 4763–4768. [CrossRef] [PubMed]
3. Baxter, P.N.W.; Khoury, R.G.; Lehn, J.M.; Baum, G.; Fenske, D. Adaptive self-assembly: Environment-induced formation and reversible switching of polynuclear metallocyclophane. *Chem. Eur. J.* **2000**, *6*, 4140–4148. [CrossRef]
4. Baum, G.; Constable, E.C.; Fenske, D.; Housecroft, C.E.; Kulke, T. Solvent control in the formation of mononuclear and dinuclear double-helical silver(I)-2,2′:6′,2″-terpyridine complexes. *Chem. Commun.* **1998**, 2659–2660. [CrossRef]
5. Mamula, O.; Lama, M.; Stoeckli-Evans, H.; Shova, S. Switchable Chiral Architectures Containing PrIII Ions: An Example of Solvent-Induced Adaptive Behavior. *Angew. Chem. Int. Ed.* **2006**, *45*, 4940–4944. [CrossRef] [PubMed]
6. Funeriu, D.P.; Lehn, J.M.; Fromm, K.M.; Fenske, D. Multiple Expression of Molecular Information: Enforced Generation of Different Supramolecular Inorganic Architectures by Processing of the Same Ligand Information through Specific Coordination Algorithms. *Chem. Eur. J.* **2000**, *6*, 2103–2111. [CrossRef]

7. Funeriu, D.P.; Rissanen, K.; Lehn, J.M. Dominant/recessive behavior in the expression of molecular information: Self-assembly of inorganic macrocyclic architectures containing coordinatively unsaturated ligands. *Proc. Natl. Acad. Sci. USA* **2001**, *98*, 10546–10551. [CrossRef]
8. Barboiu, M.; Lehn, J.M. Dynamic chemical devices: Modulation of contraction/extension molecular motion by coupled-ion binding/pH change-induced structural switching. *Proc. Natl. Acad. Sci. USA* **2002**, *99*, 5201–5206. [CrossRef]
9. Stadler, A.M.; Kyritsakas, N.; Lehn, J.M. Reversible folding/unfolding of linear molecular strands into helical channel-like complexes upon proton-modulated binding and release of metal ions. *Chem. Commun.* **2004**, 2024–2025. [CrossRef]
10. Ramírez, J.; Stadler, A.M.; Kyritsakas, N.; Lehn, J.M. Solvent-modulated reversible conversion of a [2×2]-grid into a pincer-like complex. *Chem. Commun.* **2007**, 237–239. [CrossRef]
11. Ramírez, J.; Stadler, A.M.; Brelot, L.; Lehn, J.M. Coordinative, conformational and motional behaviour of triazine-based ligand strands on binding of Pb(II) cations. *Tetrahedron* **2008**, *64*, 8402–8410. [CrossRef]
12. Ramírez, J.; Stadler, A.M.; Harrowfield, J.M.; Brelot, L.; Huuskonen, J.; Rissanen, K.; Allouche, L.; Lehn, J.M. Coordination Architectures of Large Heavy Metal Cations (Hg^{2+} and Pb^{2+}) with Bis-tridentate Ligands: Solution and Solid-State Studies. *Z. Anorg. Allg. Chem.* **2007**, *633*, 2435–2444. [CrossRef]
13. Soliman, S.M.; El-Faham, A.; Elsilk, S.E.; Farooq, M. Two heptacoordinated manganese(II) complexes of giant pentadentate s-triazine *bis*-Schiff base ligand: Synthesis, crystal structure, biological and DFT studies. *Inorg. Chim. Acta* **2018**, *479*, 275–285. [CrossRef]
14. Soliman, S.M.; El-Faham, A. Synthesis and structure diversity of high coordination number Cd(II) complexes of large *s*-triazine *bis*-Schiff base pincer chelate. *Inorg. Chim. Acta* **2019**, *488*, 131–140. [CrossRef]
15. Soliman, S.M.; El-Faham, A. Synthesis and structural DFT studies of Ni(II) and Co(II) complexes with *s*-triazine-based di-compartmental ligand. *Polyhedron* **2019**, *165*, 162–170. [CrossRef]
16. Rikagu Oxford Diffraction. *CrysAlisPro*; Agilent Technologies Inc.: Yarnton, Oxfordshire, UK, 2013.
17. Sheldrick, G.M. Crystal structure determination with SHELXL. *Acta Cryst. C* **2015**, *71*, 3–8. [CrossRef]
18. Dolomanov, O.V.; Bourhis, L.J.; Gildea, R.J.; Howard, J.A.K.; Puschmann, H. OLEX2: A complete structure solution, refinement and analysis program. *J. Appl. Cryst.* **2009**, *42*, 339–341. [CrossRef]
19. Turner, M.J.; McKinnon, J.J.; Wolff, S.K.; Grimwood, D.J.; Spackman, P.R.; Jayatilaka, D.; Spackman, M.A. Crystal Explorer 17. University of Western Australia: Crawley, Australia, 2017. Available online: http://hirshfeldsurface.net (accessed on 1 September 2019).
20. Frisch, M.J.; Trucks, G.W.; Schlegel, H.B.; Scuseria, G.E.; Robb, M.A.; Cheeseman, J.R.; Scalmani, G.; Barone, V.; Mennucci, B.; Petersson, G.A.; et al. *GAUSSIAN 09. Revision A02*; Gaussian Inc.: Wallingford, CT, USA, 2009.
21. Dennington, R., II; Keith, T.; Millam, J. *GaussView, Version 4.1*; Semichem Inc.: Shawnee Mission, KS, USA, 2007.
22. Adamo, C.; Barone, V. Exchange functionals with improved long-range behavior and adiabatic connection methods without adjustable parameters: The mPW and mPW1PW models. *J. Chem. Phys.* **1998**, *108*, 664–675. [CrossRef]
23. Glendening, E.D.; Reed, A.E.; Carpenter, J.E.; Weinhold, F. *NBO Version 3.1, CI*; University of Wisconsin: Madison, WI, USA, 1998.
24. Lu, T.; Chen, F. Multiwfn: A multifunctional wavefunction analyzer. *J. Comput. Chem.* **2012**, *33*, 580–592. [CrossRef]
25. Balouiri, M.; Sadiki, M.; Ibnsouda, S.K. Methods for *in vitro* evaluating antimicrobial activity: A review. *J. Pharm. Anal.* **2016**, *6*, 71–79. [CrossRef]
26. Barry, A.L.; Thornsberry, C. Susceptibility testing. In *Manual of Clinical Microbiology*; Lennette, E.H., Balows, A., Hausler, W.J., Truant, J.P., Eds.; American Society for Microbiology: Washington, DC, USA, 1980; pp. 561–574.
27. Singh, V.P.; Gupta, P. Synthesis and physico-chemical studies of metal(II) complexes with diacetyl benzaldehyde acyldihydrazones and their bio-activity. *J. Coord. Chem.* **2008**, *61*, 3922–3933. [CrossRef]
28. Chohan, Z.H. Ni(II), Cu(II) and Zn(II) metal chelates with some thiazole derived Schiff-bases: Their synthesis, characterization and bactericidal properties. *Met. Based Drugs* **1999**, *6*, 75–80. [CrossRef] [PubMed]
29. Azam, F.; Singh, S.; Khokhra, S.L.; Prakash, O. Synthesis of Schiff bases of naphtha[1,2-d]thiazol-2-amine and metal complexes of 2-(2′-hydroxy)benzylideneaminonaphthothiazole as potential antimicrobial agents. *J. Zhejiang Univ. Sci. B* **2007**, *8*, 446–452. [CrossRef] [PubMed]

30. Luo, W.; Meng, X.G.; Xiang, J.F.; Duan, Y.; Cheng, G.Z.; Ji, Z.P. Synthesis, characterization and bioactivity of four novel trinuclear copper(II) and nickel(II) complexes with pentadentate ligands derived from N-acylsalicylhydrazide. *Inorg. Chim. Acta* **2008**, *361*, 2667–2676. [CrossRef]
31. Bader, R.F.W. *Atoms in Molecules: A Quantum Theory*; Oxford University Press: Oxford, UK, 1990.
32. Matta, C.F.; Hernandez-Trujillo, J.; Tang, T.H.; Bader, R.F.W. Hydrogen-hydrogen bonding: A stabilizing interaction in molecules and crystals. *Chem. Eur. J.* **2003**, *9*, 1940–1951. [CrossRef]
33. Grabowski, S.J.; Pfitzner, A.; Zabel, M.; Dubis, A.T.; Palusiak, M. Intramolecular H–H interactions for the Crystal Structures of [4-((E)-But-1-enyl)-2,6- dimethoxyphenyl]pyridine-3-carboxylate and [4-((E)-Pent-1-enyl)-2,6- dimethoxyphenyl]pyridine-3-carboxylate; DFT calculations on modeled styrene derivatives. *J. Phys. Chem. B* **2004**, *108*, 1831–1837. [CrossRef]
34. Matta, C.F.; Castillo, N.; Boyd, R.J. Characterization of a closed-shell fluorine-fluorine bonding interaction in aromatic compounds on the basis of the electron density. *J. Phys. Chem. A* **2005**, *109*, 3669–3681. [CrossRef]
35. Pendás, A.M.; Francisco, E.; Blanco, M.A.; Gatti, C. Bond paths as privileged exchange channels. *Chem. Eur. J.* **2007**, *13*, 9362–9371. [CrossRef]
36. Bobrov, M.F.; Popova, G.V.; Tsirelson, V.G. A topological analysis of electron density and chemical bonding in cyclophosphazenes $P_nN_nX_{2n}$ (X = H, F, Cl; n = 2, 3, 4). *Russ. J. Phys. Chem.* **2006**, *80*, 584–590. [CrossRef]
37. Gatti, C. Chemical bonding in crystals: New directions. *Z. Kristallogr.* **2005**, *220*, 399–457. [CrossRef]
38. Gibbs, G.V.; Downs, R.T.; Cox, D.F.; Ross, N.L.; Boisen, M.B., Jr.; Rosso, K.M. Shared and closed-shell O-O interactions in silicates. *J. Phys. Chem. A* **2008**, *112*, 3693–3699. [CrossRef] [PubMed]
39. Espinosa, E.; Molins, E.; Lecomte, C. Hydrogen bond strengths revealed by topological analyses of experimentally observed electron densities. *Chem. Phys. Lett.* **1998**, *285*, 170–173. [CrossRef]